Mechanistic Insights into $NO_3^\bullet$ Induced Self-Terminating Radical Oxygenations, Part 1: A Computational Study on $NO_3^\bullet$ and Its Addition to Alkynes

Uta Wille*,†,‡ and Tim Dreessen†,§

School of Chemistry, The University of Melbourne, Victoria 3010, Australia, BIO21 Molecular Science and Biotechnology Institute, 30 Flemington Road, Victoria 3010, Australia, and Otto-Diels-Institut für Organische Chemie, Universität Kiel, Olshausenstr. 40, 24098 Kiel, Germany.

Received: October 5, 2004; In Final Form: December 5, 2005

The geometry of the nitrate radical, $NO_3^\bullet$, for which unrestricted Hartree−Fock (HF) breaks spatial symmetry of the wave function, was optimized using hybrid density functionals that include varying fractions of Hartree−Fock exchange. Although symmetry breaking was not observed even when the functional with the highest HF exchange (BHandHLYP) was used, only B3LYP correctly describes the D_{3h} symmetry of $NO_3^\bullet$ as ground-state structure with the lowest energy. Further, geometries and energies of the stationary points in the addition of $NO_3^\bullet$ to ethyne, propyne, and 2-butyne were calculated using ab initio and density functional methods. The reactions proceed through *Z*-configurated transition states leading to *Z*-configurated vinyl radicals with the activation barrier decreasing with increasing methyl substitution at the C≡C triple bond by ca. 11 kJ mol^{-1} per methyl group. It was found that the results obtained at the BHandHLYP/cc-pVDZ level of theory are in good agreement with the data from single-point QCISD and CCSD(T) calculations.

Introduction

The electrophilic nitrate radical, $NO_3^\bullet$, is an important atmospheric free radical and is mainly responsible for the chemical transformations in the nighttime troposphere.[1] We recently demonstrated that $NO_3^\bullet$ is also a versatile reagent in organic synthesis that can be used as an *O*-atom synthon to transform C≡C triple bonds into carbonyl compounds through a diastereoselective, oxidative radical addition−cyclization cascade ("self-terminating radical oxygenations").[2,3] Since experimental mechanistic investigations of such complex radical reactions are difficult to perform because of short lifetimes and low concentrations of intermediates, we decided to study this radical oxygenation with computational methods in order to gain insight into the energetics and driving forces of this reaction sequence. This paper presents the results of our computational studies on the initial reaction step, e.g., the addition of $NO_3^\bullet$ to alkynes.[4] As the size of the molecules in this radical oxygenation (at least 12 carbon atoms) seriously limits the applicable computational methods in terms of required CPU time, one major aim of this work is to reveal a reliable and computationally cost-efficient method that will enable us to study the entire mechanism of $NO_3^\bullet$ induced self-terminating radical oxygenations in the future.

Despite its small size, $NO_3^\bullet$ is a very challenging species for computational chemists. Numerous experimental and theoretical studies were performed to determine the gas-phase structure of $NO_3^\bullet$ that could be either of Y-shaped C_{2v} or of planar trigonal D_{3h} geometry.[1] Most early quantum chemical investigations resulted in a C_{2v} ground-state geometry with two short and one long N−O bonds,[5] whereas experiments are more consistent with D_{3h} symmetric $NO_3^\bullet$.[6] Many of these theoretical studies, however, did not pay any or only a little attention to the frequent symmetry breaking of the electronic wave function of highly symmetric molecules such as $NO_3^\bullet$, which may have led to the incorrect C_{2v} geometry.[7] A recent ab initio study revealed that symmetry breaking in $NO_3^\bullet$ computations could be avoided by inclusion of static and dynamic electron correlation,[8] but such computationally highly demanding methods are not applicable to our intended study of the entire mechanism of $NO_3^\bullet$ induced self-terminating radical oxygenations.

In recent years, density functional theory (DFT) has become very popular, as it is less computationally intensive than other methods with similar accuracy. Because of its nature, occurrence of symmetry breaking should be less probable, and all calculations based on pure DFT yielded a D_{3h} symmetric electronic ground state of $NO_3^\bullet$.[9] Computations using density functionals with local exchange functionals, for example, SVWN,[10,11] led to satisfactory geometries for $NO_3^\bullet$ but calculated both poor frequencies and poor energies, resulting in negative values for the heat of formation, $\Delta_f H°$.[9b] Methods with nonlocal exchange functionals, e.g., BLYP,[12,13] BP86,[14] and BPW91,[15] generally led to geometries with bond lengths that were too long.[9] The calculated energies were better than those obtained using SVWN, however, still not in accordance with experimental values.[16] Of all DFT methods studied to date, the results obtained using the hybrid density functionals B3P86, B3PW91, and B3LYP[13−15,17] were in the best agreement with the experimental data of ground-state $NO_3^\bullet$.

A general problem encountered with hybrid DFT methods is the frequent underestimation of energy barriers in radical reactions, which could be overcome by using hybrid density functionals with a higher Hartree−Fock (HF) exchange.[18] Recently applied methods of this type are BHandHLYP,[19] that differs from B3LYP by a 50% HF exchange instead of 20%, mPW1PW91,[20] with 25% HF exchange, and mPW1K,[21] with 43% HF exchange. To our knowledge, a systematic study of the influence of HF exchange in hybrid functionals on $NO_3^\bullet$

* Corresponding author. Email: uwille@unimelb.edu.au.
† The University of Melbourne.
‡ BIO21 Molecular Science and Biotechnology Institute.
§ Otto-Diels-Institut für Organische Chemie.

10.1021/jp0454772 CCC: $33.50
Published on Web 01/26/2006

SCHEME 1

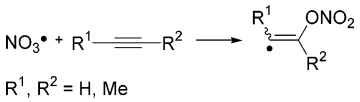

geometry, energy, and symmetry breaking does not exist. In the first section of this paper, we will therefore present the performance of currently used hybrid DFT methods with various degrees of HF exchange, in combination with different basis sets, to calculate $NO_3^•$.

Whereas the reactions of $NO_3^•$ with alkenes have been extensively investigated both experimentally[1] and theoretically,[22] $NO_3^•$ addition to alkynes, the initial step in self-terminating radical oxygenations, has attracted far less attention and, to our knowledge, has never been studied with computational methods.[1,23] In the second part of this paper, the results of our ab initio and DFT calculations on the reaction of $NO_3^•$ with small un-, mono-, and disubstitued alkynes, e.g., ethyne, propyne, and 2-butyne, will be presented (Scheme 1).

Theoretical Methods

A. $NO_3^•$ Calculations. Geometry optimizations were performed for D_{3h} and C_{2v} symmetries of $NO_3^•$ using the software package *Gaussian 98*[24b,c] with the hybrid functionals B3LYP, mPW1PW91, mPW1K,[21] and BHandHLYP, in combination with the 6-311G*, 6-311+G*, cc-pVDZ, and aug-cc-pVDZ basis sets. In the case of a C_{2v} symmetric wave function, nonequivalent Mulliken charges for one of the three oxygen atoms in $NO_3^•$ and a significant dipole moment would be expected, whereas $NO_3^•$ with D_{3h} symmetry should have equal atomic charges and no dipole moment. Spatial symmetry breaking of the wave function would be diagnosed by the presence of nonequivalent atomic charges for symmetry-equivalent atoms. Frequency analyses and wave function stability tests, as implemented in Gaussian, were carried out for all optimized geometries. The spin expectation value, $\langle s^2 \rangle$, never exceeded 0.763 in these computations.

B. Calculations of the $NO_3^•$ Addition to Alkynes. The computations were performed with the software packages *Gaussian 94*, *98*, and *03*.[24] Geometry optimizations were performed at the UHF/6-311G**, B3LYP/6-311G**, B3LYP/cc-pVDZ, mPW1PW91/6-311G**, mPW1K/6-31+G**,[21] BHandHLYP/6-311G**, BHandHLYP/cc-pVDZ, BHandHLYP/cc-pVTZ, and BHandHLYP/aug-cc-pVTZ levels of theory. QCISD/cc-pVDZ and CCSD(T)/cc-pVDZ single-point calculations were performed on all BHandHLYP/aug-cc-pVTZ optimized geometries. Additional single-point calculations were also performed at the QCISD/aug-cc-pVDZ and CCSD(T)/aug-cc-pVDZ levels of theory on selected B3LYP/aug-cc-pVDZ optimized structures. Frequency analyses were carried out for all optimized ground- and transition-state geometries. Intrinsic reaction coordinate (IRC) calculations for all transition states were performed at the BHandHLYP/6-311G** level of theory. Tables with electronic energies, $\langle s^2 \rangle$ values, imaginary frequencies of transition states, ν_{imag}, and selected geometrical parameters computed at all levels of theory are given in the electronic Supporting Information.

Results and Discussion

A. $NO_3^•$ Calculations. Table 1 shows the calculated geometrical data (see Figure 1 for labeling), energy differences, atomization energies, heats of formation, $\Delta_f H°$, and selected harmonic frequencies for the C_{2v} and D_{3h} symmetries of $NO_3^•$. The computed electronic energies, Mulliken charges, dipole moments, μ_z, and the remaining harmonic frequencies of $NO_3^•$ are available as electronic Supporting Information.

In all calculations, the electronic ground state was found to be $^2B_2$ for C_{2v} and $^2A_2'$ for D_{3h} symmetric $NO_3^•$. Computations using the mPW1PW91 functional revealed a third $NO_3^•$ geometry with "inverted" C_{2v} symmetry possessing two long and one short N−O bonds (denoted C'_{2v}; see Figure 1).

By comparison with the experimental data,[6c] all computational methods resulted in bond lengths r_1-r_3 that were slightly too short. In the B3LYP calculations, the bond lengths for both geometries varied only in the fourth decimal place. Thus, geometry assignments were made from the calculated Mulliken charges that occasionally showed a minimal inequality between the charges of O^1/O^2 and O^3, resulting in a minute dipole moment that would formally correspond to a C_{2v} symmetry (see Supporting Information). We suggest that both structures should be considered the same, namely D_{3h} that is slightly lower in energy by ca. 0.03−0.04 kJ mol^{-1}.[25]

In all cases, Mulliken charges and dipole moments were in accordance with the respective calculated geometry (see Supporting Information), indicating that no spatial symmetry breaking of the wave function occurred, not even in the case of the hybrid density functional with the highest HF exchange under investigation (BHandHLYP). From the energy difference between D_{3h} and C_{2v} symmetry, ΔE, it turned out that only computations using the B3LYP functional led to a D_{3h} symmetry as the lowest-energy structure of $NO_3^•$ (see above), whereas mPW1K and BHandHLYP calculated a significantly more stable C_{2v} geometry. Albeit the energy differences are only small, the mPW1PW91 computations revealed the inverted C'_{2v} structure as the energetically most favorable geometry of $NO_3^•$, whereas D_{3h} and C_{2v} are practically identical and slightly higher in energy. So far, such a C'_{2v} geometry of $NO_3^•$ was only found in CASSCF calculations, but, in contrast to our results, as a transition state between two equivalent minima of C_{2v}.[26]

Examination of the harmonic frequencies revealed that density functionals with higher HF exchange than in B3LYP calculate imaginary frequencies for the degenerate in-plane bend, e', in D_{3h} symmetric $NO_3^•$, so that this geometry must be considered a saddle point of second order. As was shown by both theoretical and experimental studies, this frequently encountered complication in $NO_3^•$ calculations is probably due to strong interactions (i.e., pseudo-Jahn−Teller-effect) between the $^2A_2'$ ground state and the second excited state $^2E'$.[6h,8,27] Such a second-order saddle point was also found for the D_{3h} symmetry in the mPW1K/6-311G* calculations. Surprisingly, the computations performed at the mPW1K/6-311+G* level of theory resulted in a D_{3h} minimum, which is, however, ca. 14 kJ mol^{-1} higher in energy than its C_{2v} counterpart. At present, we have no explanation for this strong influence of diffuse functions on the outcome.[28]

All mPW1PW91 computations showed an imaginary frequency of the asymmetric b_2 mode in C_{2v} symmetric $NO_3^•$ so that this geometry must be considered a transition state of the pseudorotation between two equivalent minima of the "inverted" structure C'_{2v}.

A very strong method-dependent outcome was also observed for the atomization energy and the heat of formation at 298.15 K, $\Delta_f H°$.[29] Whereas hybrid functionals with lower HF exchange (B3LYP and mPW1PW91) led to results being in satisfactory accordance with experimental data,[9b,16] the higher HF exchange in mPW1K and BHandHLYP gave significantly underestimated atomization energies and thus values for $\Delta_f H°$ that were too high.

TABLE 1: Calculated Geometries, Energy Differences, ΔE, Atomization Energies, Heats of Formation, $\Delta_f H°$, and Selected Harmonic Frequencies (unscaled) for C_{2v} and D_{3h} Symmetric $NO_3^•$

		geometry						asymmetric bend[e]	
method	sym.	$r_{1,2}$/Å	r_3/Å	α/°	ΔE[a,b]	atom. energy[b,c]	$\Delta_f H°$[b,d]	$a_1(e')$	$b_2(e')$
				B3LYP					
6-311G*	C_{2v}	1.233(2)	1.233(1)	119.9	$-0.0_{(3)}$	1137	43.8	256	262
6-311G*	D_{3h}	1.233(2)	1.233(2)	120.0		1137	43.8	259	259
cc-pVDZ	C_{2v}	1.235(1)	1.235(4)	120.0	$-0.0_{(3)}$	1150	30.9	240	240
cc-pVDZ	D_{3h}	1.235(4)	1.235(4)	120.0		1150	30.8	239	239
6-311+G*	C_{2v}	1.233(6)	1.234(2)	120.1	$-0.0_{(3)}$	1124	57.0	287	283
6-311+G*	D_{3h}	1.234(1)	1.234(1)	120.0		1124	57.0	284	284
aug-cc-pVDZ	C_{2v}	1.236(8)	1.237(1)	120.0	$-0.0_{(4)}$	1146	35.4	260	258
aug-cc-pVDZ	D_{3h}	1.237(1)	1.237(1)	120.0		1146	35.3	258	258
				mPW1PW91					
6-311G*	C_{2v}	1.215	1.241	123.4	0.3[f]	1115	67.5	279	252i
6-311G*	C'_{2v}	1.239	1.198	113.1	$0.0_{(2)}$	1112	69.5	317	394
6-311G*	D_{3h}	1.223	1.223	120.0		1117	66.8	226i	226i
cc-pVDZ	C_{2v}	1.217	1.245	123.8	0.5[f]	1122	60.7	313	279i
cc-pVDZ	C'_{2v}	1.243	1.199	112.3	$0.0_{(2)}$	1119	62.7	331	433
cc-pVDZ	D_{3h}	1.225	1.225	120.0		1124	59.6	238i	238i
6-311+G*	C_{2v}	1.217	1.240	123.0	0.1[f]	1106	76.3	248	209i
6-311+G*	C'_{2v}	1.237	1.202	114.4	0.0	1104	77.5	271	324
6-311+G*	D_{3h}	1.224	1.224	120.0		1108	75.9	192i	192i
aug-cc-pVDZ	C_{2v}	1.219	1.245	123.4	0.3[f]	1128	54.8	275	256i
aug-cc-pVDZ	C'_{2v}	1.243	1.203	112.8	$0.0_{(2)}$	1125	56.7	313	397
aug-cc-pVDZ	D_{3h}	1.227	1.227	120.0		1129	54.1	224i	224i
				mPW1K					
6-311G*	C_{2v}	1.185	1.306	130.6	14.1	972	209.6	667	228
6-311G*	D_{3h}	1.209	1.209	120.0		964	219.6	79i	79i
cc-pVDZ	C_{2v}	1.187	1.305	130.8	13.8	974	207.4	656	178
cc-pVDZ	D_{3h}	1.211	1.211	120.0		966	217.8	113i	114i
6-311+G*	C_{2v}	1.185	1.307	130.5	13.9	968	214.4	664	268
6-311+G*	D_{3h}	1.210	1.210	120.0		959	220.5	77	77
aug-cc-pVDZ	C_{2v}	1.190	1.304	130.7	13.5	990	191.6	644	200
aug-cc-pVDZ	D_{3h}	1.213	1.213	120.0		982	201.5	109i	109i
				BHandHLYP					
6-311G*	C_{2v}	1.184	1.326	131.3	26.2	871	311.2	703	429
6-311G*	D_{3h}	1.210	1.210	120.0		859	324.4	2787i	2786i
cc-pVDZ	C_{2v}	1.186	1.326	131.4	26.1	876	307.0	698	406
cc-pVDZ	D_{3h}	1.212	1.212	120.0		863	320.3	2798i	2798i
6-311+G*	C_{2v}	1.184	1.327	131.2	25.6	866	316.9	702	446
6-311+G*	D_{3h}	1.211	1.211	120.0		854	329.4	2771i	2770i
aug-cc-pVDZ	C_{2v}	1.189	1.324	131.3	25.1	887	295.6	696	414
aug-cc-pVDZ	D_{3h}	1.214	1.214	120.0		876	307.9	2766i	2765i
experiment	D_{3h}	1.240[g]	1.240[g]	120.0[g]		1150[h]	73.7[i]	363[j]	363[j]

[a] Energy difference $\Delta E = E(D_{3h}) - E(C_{2v})$. [b] In kJ mol^{-1}. [c] ZPE correction included. [d] At 298.15 K. [e] In cm^{-1}. [f] Energy difference $\Delta E = E(D_{3h}) - E(C'_{2v})$. [g] ref 6c. [h] ref 9b. [i] ref 16. [j] ref 6c,g.

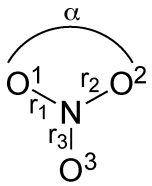

Figure 1.

From these findings, it can be concluded that, out of the set of hybrid density functionals studied in this work, the results of the B3LYP computations are in the best agreement with the experimental values for $NO_3^•$, whereas the mPW1PW91, mPW1K, and BHandHLYP methods are leading to a wrong ground-state geometry for this radical.

B. Reaction of $NO_3^•$ with Alkynes. *Ethyne.* Addition of $NO_3^•$ to ethyne proceeds via initial formation of a prereactive association complex (**complex-e**) with an $NO_3^•$−ethyne distance of ca. 3.5 Å through two different transition states, **TS-e(s)** and **TS-e(a)**, leading to four vinyl radicals with either *E* [***E*-e(s)**, ***E*-e(a)**] or *Z* configuration [***Z*-e(s)**, ***Z*-e(a)**] at the C═C double bond.[30]

Figure 2 shows the stationary points and selected geometrical data calculated at the BHandHLYP/cc-pVDZ, BHandHLYP/aug-cc-pVTZ, and B3LYP/cc-pVDZ levels of theory (for further data, see electronic Supporting Information). The energies of the stationary points on the reaction coordinate (Figure 3) relative to the reactants $NO_3^•$ and ethyne are compiled in Table 2.

The potential symmetry breaking in UHF calculations of $NO_3^•$ and the fact that all hybrid density functionals used in this work, except B3LYP, are computing a wrong ground-state $NO_3^•$ geometry, might both give rise to incorrect reference energies. An $NO_3^•$−ethyne "supermolecule" with a distance of ca. 20 Å between $NO_3^•$ and alkyne was therefore calculated (not shown) and taken as the zero-energy reference.[31] This procedure had a major impact on the results of the UHF/6-311G** calculations, where energy differences of up to 100 kJ mol^{-1} were obtained between computations using the supermolecule or the sum of

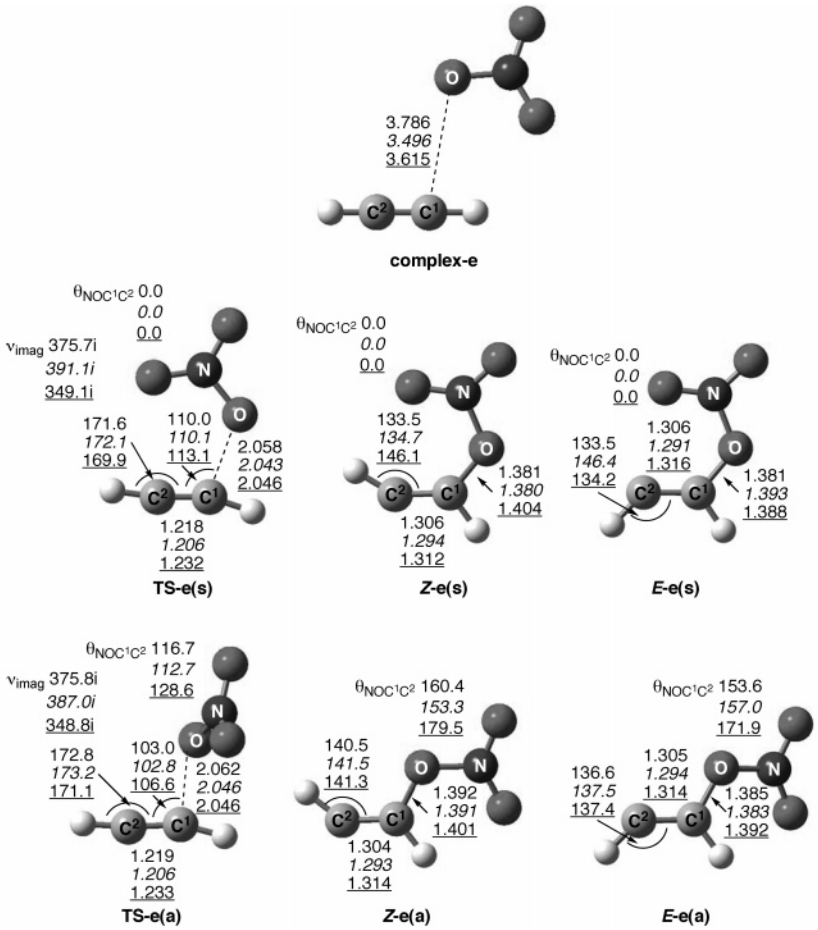

Figure 2. Geometrical data (bond distances in Å, angles and dihedral angles (θ) in deg) and imaginary frequencies (ν_{imag}) of the stationary points of the addition of $NO_3^\bullet$ at ethyne (normal, BHandHLYP/cc-pVDZ; italics, BHandHLYP/aug-cc-pVTZ; underlined, B3LYP/cc-pVDZ).

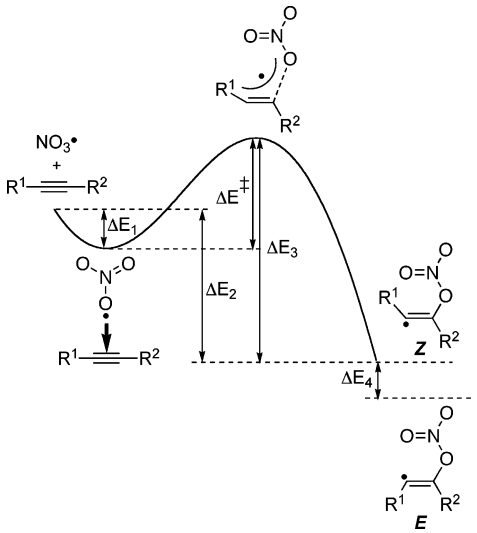

Figure 3. Potential surface of the $NO_3^\bullet$ addition to alkynes (for the sake of clarity, partial charges are omitted).

the electronic energies of the reactants as reference energy value. On the other hand, consideration of a supermolecule in exemplary performed B3LYP and BHandHLYP computations turned out to be not necessary as the resulting energies differed by only max. 0.3 kJ mol^{-1} from those using the energy of the reactants as zero-energy reference.

According to the DFT calculations, the activation energy, $\Delta E^\ddagger$, for addition through transition state **TS-e(a)**, in which the nitrate moiety is twisted out of the plane of the carbon framework (angular, a), is ca. 3 kJ mol^{-1} below that required for the pathway via transition state **TS-e(s)**, in which $NO_3^\bullet$ attacks ethyne in a *syn* (s) periplanar fashion. The attacking angle of the radical at the C≡C triple bond is with ca. 103° [**TS-e(a)**] or 110° [**TS-e(s)**], respectively, in the same order of magnitude as in radical additions to alkenes.[32] Except for the relative orientation of the nitrate group, the geometries of both transition states are very similar. The comparatively large distance of ca. 2.05 Å between $NO_3^\bullet$ and the attacked carbon C^1 in **TS-e(a/s)** and a π bond elongation by only ca. 0.02 Å, compared to the C≡C triple bond in ethyne (data not shown), indicate an early transition state. Both transition states have *Z* configuration, and are leading, according to IRC calculations, to the *Z*-configurated vinyl radicals ***Z*-e(a)** and ***Z*-e(s)**, respectively, which also possess either an angular or syn arrangement of the nitrate group relative to the vinyl moiety. The angular configurated ***Z*-e(a)** is slightly more stable by ca. 4−6 kJ mol^{-1} than its syn counterpart ***Z*-e(s)**. The *E*-configurated vinyl radicals ***E*-e(a)** and ***E*-e(s)** are energetically very similar to ***Z*-e(a)**/***Z*-e(s)**[25] and should be accessible through *Z*/*E* inversion that requires only a few kilojoules per mole of activation energy.[33] The unpaired electron in ***Z*/*E*-e(a/s)** is located in an sp^2 orbital, as is expected for nonlinear, σ-type vinyl radicals. The exemplary selected geometrical parameters obtained from calculations at different levels of theory (Figure 2) show only small variations. It was satisfying to see that computationally expensive basis sets and inclusion of diffuse functions (e.g., aug-cc-pVTZ) do not lead to an entirely different outcome. The only exemption from this was the dihedral angle $\theta_{NOC^1C^2}$ in the

TABLE 2: Relative Energies (in kJ mol^{-1}) for the Addition of $NO_3^\bullet$ to Ethyne[a,b]

		syn pathway				angular pathway			
method	ΔE_1	$\Delta E^\ddagger$	ΔE_2	ΔE_3	ΔE_4	$\Delta E^\ddagger$	ΔE_2	ΔE_3	ΔE_4
UHF/	−4.5	69.5	−59.4	124.4	−0.2	70.6	−70.1	136.2	0.8
6-311G**[c]	*−3.2*	*62.4*	*−49.3*	*108.5*	*0.8*	*66.3*	*−60.1*	*123.2*	*1.0*
B3LYP/	−5.1	22.5	−63.4	80.8	−0.2	19.3	−73.8	82.0	−0.9
6-311G**	*−2.6*	*29.5*	*−45.5*	*72.4*	*0.5*	*26.4*	*−50.2*	*74.0*	*−0.7*
B3LYP/	−9.3	21.6	−79.0	91.3	0.8	18.4	−83.4	92.5	−1.0
cc-pVDZ	*−6.1*	*27.7*	*−60.9*	*82.5*	*1.5*	*24.2*	*−65.6*	*83.7*	*−0.5*
B3LYP/	−2.2	19.4	−67.6	84.8	0.6	14.9	−73.8	86.5	0.1
aug-cc-pVDZ	*0.4*	*26.8*	*−48.4*	*75.6*	*1.4*	*22.2*	*−55.0*	*77.6*	*0.5*
mPW1PW91/	−5.2	17.8	−89.2	101.8	−0.1	14.4	−93.8	103.0	−0.6
6-311G**	*−3.0*	*23.9*	*−71.5*	*92.4*	*0.6*	*20.6*	*−76.5*	*94.1*	*−0.4*
mPW1K/	−4.0	13.8	−112.8	122.6	−1.0	10.6	−118.1	124.7	0.4
6-31+G**	*−2.0*	*16.1*	*−97.5*	*111.6*	*−0.2*	*13.0*	*−103.4*	*114.4*	*0.7*
BHandHLYP/	−6.4	23.1	−88.4	105.1	−1.3	20.9	−93.1	107.6	−0.1
6-311G**	*−4.6*	*25.0*	*−74.7*	*95.1*	*−0.6*	*22.8*	*−79.7*	*97.9*	*0.1*
BHandHLYP/	−9.0	20.6	−102.9	114.5	−0.4	18.6	−107.3	116.9	−0.2
cc-pVDZ	*−6.6*	*21.7*	*−88.9*	*104.0*	*0.2*	*19.5*	*−93.9*	*106.8*	*0.1*
BHandHLYP/	−4.4	26.4	−85.9	107.9	−0.7	23.3	−91.8	110.7	0.7
cc-pVTZ	*−2.9*	*28.6*	*−72.0*	*97.7*	*0.1*	*25.4*	*−78.2*	*100.7*	*1.0*
BHandHLYP/	−3.3	26.0	−84.1	106.8	−0.6	22.8	−90.0	109.5	1.2
aug-cc-pVTZ	*−1.5*	*27.6*	*−70.4*	*96.5*	*0.2*	*24.4*	*76.7*	*99.6*	*1.4*
QCISD/cc-pVDZ[d]	−8.8	46.7	−74.7	112.6	0.2	44.2	−79.6	115.0	−0.7
CCSD(T)/cc-pVDZ[d]	−10.1	36.6	−84.0	110.6	0.2	33.9	−88.8	112.6	−0.9
QCISD/aug-cc-pVDZ[e]				108.1	0.0			108.6	0.7
CCSD(T)/aug-cc-pVDZ[e]				106.1	0.4			107.1	0.3

[a] In italics: ZPE included. [b] Energies relative to ethyne and $NO_3^\bullet$ calculated at the same level of theory. [c] Energies relative to an ethyne−$NO_3^\bullet$ supermolecule (see text), calculated at UHF/6-311G**. [d] Single-point calculation on BHandHLYP/aug-cc-pVTZ optimized geometry. [e] Single-point calculation on B3LYP/aug-cc-pVDZ optimized geometry.

vinyl radicals ***Z***/***E*-e(a)**, where B3LYP/cc-pVDZ calculates a more linear arrangement than the BHandHLYP method.

In contrast to this, the UHF/6-311G** calculations did not reveal a planar *syn*-configurated transition state, but only structures in which the nitrate moiety is twisted out of the plane of the ethyne framework (see Supporting Information). In addition, significantly higher activation barriers and smaller reaction enthalpies, ΔE_2, were obtained. As the UHF calculations are burdened with generally very large spin contamination even after annihilation, these results can be taken as another example of the poor ability of this method to interpret the reactions of open-shell species.

Examination of the energy difference ΔE_3 between the transition state and the respective *Z*-configurated vinyl radical reveals that the QCISD and CCSD(T) single-point calculations give the same relative positions of transition state and *Z*- and *E*-configurated vinyl radical with differences of less than 2.6 kJ mol^{-1}. To our satisfaction, the computed single-point energies showed no dependence on the level of theory that was used to optimize the geometries (B3LYP/aug-cc-pVDZ and BHandHLYP/aug-cc-pVTZ) and also not on the basis set employed in the single-point calculations (cc-pVDZ and aug-cc-pVDZ, respectively). We have therefore taken the ΔE_3 value, which corresponds to the activation barrier of the reverse fragmentation of the vinyl radical into $NO_3^\bullet$ and ethyne, to benchmark the performance of the various DFT methods used in this work.[34] Thus, the B3LYP results converge toward a ΔE_3 value that is lower by ca. 25 ± 5 kJ mol^{-1} than the QCISD and CCSD(T) values and lower by even further 10 kJ mol^{-1}, when the zero-point vibrational energy (ZPE) correction is included.[35] The mPW1PW91/6-311G** results are lower by ca. 10 kJ mol^{-1}, whereas the values from the mPW1K/6-31+G** calculations are ca. 10 kJ mol^{-1} higher, compared to the single-point calculations at correlated levels. Inclusion of the ZPE correction has a larger effect on the B3LYP and mPW1PW91 computations by increasing the activation barrier $\Delta E^\ddagger$ by ca. 6 kJ mol^{-1} and reducing the reaction enthalpy ΔE_2 by ca. 19 kJ mol^{-1}. In the BHandHLYP calculations, ZPE corrections result in an insignificant increase of $\Delta E^\ddagger$ by 2 kJ mol^{-1} and a reduction of ΔE_2 by ca. 14 kJ mol^{-1}. Of all methods employed in this work, it appears that the results obtained at the BHandHLYP/cc-pVDZ level of theory are in the best agreement with the QCISD and CCSD(T) computations. Larger basis sets in combination with BHandHLYP do not lead to a significantly different outcome. In contrast to this, DFT methods with a lower HF exchange than in the BHandHLYP functional are not suitable for studying this radical addition reaction.

Propyne. Addition of $NO_3^\bullet$ at propyne proceeds, after initial formation of an intermediate prereactive complex (**complex-p**), at the less-substituted carbon (C^1) of the C≡C triple bond via the *Z*-configurated, angular transition state **TS-p** to give the likewise *Z*-configurated vinyl radical ***Z*-p** that may undergo isomerization to the vinyl radical ***E*-p** possessing *E* configuration (Figure 4).[36] The angle of radical attack in **TS-p** is slightly lower than in **TS-e(a)**, as is also the dihedral angle $\theta_{NOC^1C^2}$ in ***E*-p** and ***Z*-p** compared to ***E*/*Z*-e(a)**.[37] Planar, syn configurated structures, similar to ***E*/*Z*-e(s)** and **TS-e(s)**, were not located, which may be rationalized by increased steric interactions between the nitrate moiety and the methyl group at C^2.

Similar to the $NO_3^\bullet$/ethyne case, comparison of the energy differences between transition state and *Z*-configurated vinyl radical, ΔE_3, revealed that the results obtained from the BHandHLYP/cc-pVDZ calculations are in the best agreement with those from the single-point computations at correlated levels (Table 3).[38] All calculations show that the *Z*-configurated vinyl radical ***Z*-p** is energetically slightly more favorable by up to 2.6 kJ mol^{-1} (DFT) or up to 4.0 kJ mol^{-1} [CCSD(T)], respectively, than ***E*-p**. The activation barrier for the $NO_3^\bullet$ addition to propyne is lower by some kilojoules per mole than that calculated for the $NO_3^\bullet$/ethyne reaction (see Figure 4).

2-Butyne. Formation of an intermediate prereactive complex, **complex-b**, was also identified in the $NO_3^\bullet$ addition to 2-butyne. This reaction proceeds through a *Z*-configurated, angular transition state **TS-b** to give the angular vinyl radical ***Z*-b** that

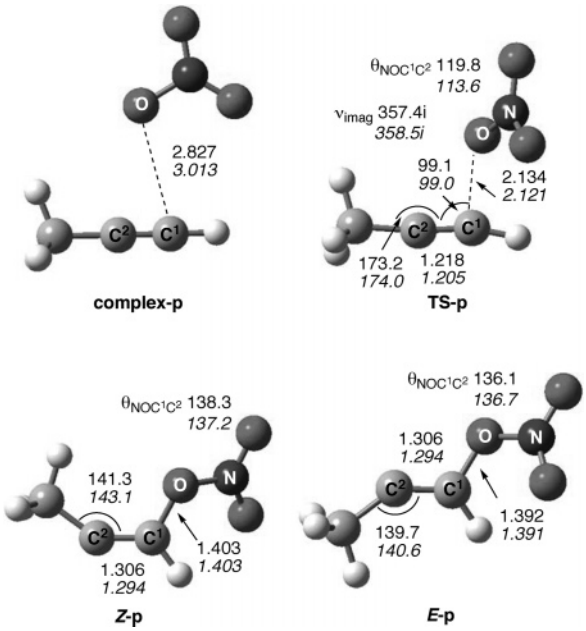

Figure 4. Geometrical data (bond distances in Å, angles and dihedral angles (θ) in deg) and imaginary frequencies (ν_{imag}) of the stationary points of the addition of $NO_3^\bullet$ at propyne (normal, BHandHLYP/cc-pVDZ; italics, BHandHLYP/aug-cc-pVTZ).

TABLE 3: Relative Energies (in kJ mol^{-1}) for the Addition of $NO_3^\bullet$ to Propyne[a,b]

method	ΔE_1	$\Delta E^\ddagger$	ΔE_2	ΔE_3	ΔE_4
BHandHLYP/6-311G**	−8.3	8.3	−99.3	99.3	−2.6
	−5.8	*9.4*	*−85.7*	*89.3*	*−1.9*
BHandHLYP/cc-pVDZ	−10.5	6.7	−112.2	108.4	−2.6
	−7.7	*7.4*	*−98.2*	*97.9*	*−1.8*
BHandHLYP/cc-pVTZ	−5.2	10.0	−96.4	102.2	−1.3
	−3.3	*11.5*	*−82.7*	*90.9*	*−0.7*
BHandHLYP/aug-cc-pVTZ	−3.5	8.6	−94.6	99.6	−0.7
	−1.7	*10.0*	*−81.1*	*89.4*	*−0.1*
QCISD/cc-pVDZ[c]	−6.2	29.1	−86.0	108.9	3.2
CCSD(T)/cc-pVDZ[c]	−8.2	19.4	−96.1	107.3	4.0
QCISD/aug-cc-pVDZ[d]				104.3	−1.6
CCSD(T)/aug-cc-pVDZ[d]				103.0	−2.3

[a] In italics: ZPE included. [b] Energies relative to propyne and $NO_3^\bullet$ calculated at the same level of theory. [c] Single-point calculation on BHandHLYP/aug-cc-pVTZ optimized geometry. [d] Single-point calculation on B3LYP/aug-cc-pVDZ optimized geometry.

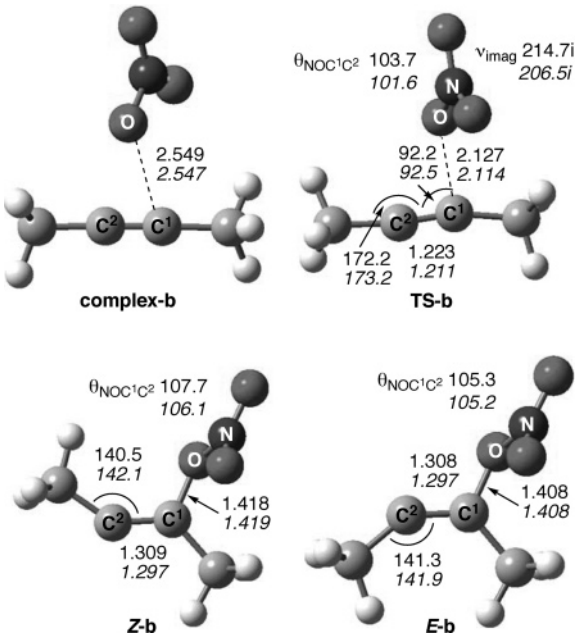

Figure 5. Geometrical data (bond distances in Å, angles and dihedral angles (θ) in deg) and imaginary frequencies (ν_{imag}) of the stationary points of the addition of $NO_3^\bullet$ at 2-butyne (normal, BHandHLYP/cc-pVDZ; italics, BHandHLYP/aug-cc-pVTZ).

TABLE 4: Relative Energies (in kJ mol^{-1}) for the Addition of $NO_3^\bullet$ to 2-Butyne[a,b]

method	ΔE_1	$\Delta E^\ddagger$	ΔE_2	ΔE_3	ΔE_4
BHandHLYP/6-311G**	−16.0	4.0	−94.2	82.2	−4.1
	−11.9	*4.1*	*−82.2*	*74.4*	*−3.9*
BHandHLYP/cc-pVDZ	−18.6	2.9	−106.2	90.5	−4.3
	−14.2	*3.0*	*−93.6*	*82.4*	*−4.0*
BHandHLYP/cc-pVTZ	−10.3	4.3	−89.4	83.4	−3.1
	−6.6	*4.8*	*−77.3*	*75.5*	*−3.0*
BHandHLYP/aug-cc-pVTZ	−9.0	3.1	−87.4	81.5	−2.5
	−5.5	*3.4*	*−75.6*	*73.5*	*−2.5*
QCISD/cc-pVDZ[c]	−0.8	12.2	−87.2	98.6	−4.7
CCSD(T)/cc-pVDZ[c]	−8.9	5.8	−99.1	96.0	−4.9
QCISD/aug-cc-pVDZ[d]				90.5	−4.0
CCSD(T)/aug-cc-pVDZ[d]				86.1	−1.8

[a] In italics: ZPE included. [b] Energies relative to 2-butyne and $NO_3^\bullet$ calculated at the same level of theory. [c] Single-point calculation on BHandHLYP/aug-cc-pVTZ optimized geometry. [d] Single-point calculation on B3LYP/aug-cc-pVDZ optimized geometry.

may undergo isomerization to give ***E*-b** (Figure 5). Similar to the situation in the $NO_3^\bullet$/propyne reaction, steric hindrance between the nitrate group and methyl substituents at C^2 may impede an in-plane syn $NO_3^\bullet$ attack at the C≡C triple bond. The calculated geometries for ***E*/*Z*-p** and **TS-p**, respectively, are very similar to those in the corresponding $NO_3^\bullet$/propyne reaction.[30] The major structural differences are the angle of radical attack in **TS-b**, which is slightly smaller (ca. 92°) compared with **TS-p** and the nearly perpendicular orientation of the nitrate moiety relative to the carbon framework in ***E*/*Z*-p**. At all levels of theory, the *Z*-configurated vinyl radical ***Z*-b** was found to be energetically favored over ***E*-b** by some 5 kJ mol^{-1} (Table 4). The activation barrier for the $NO_3^\bullet$ addition to 2-butyne is lower than found for the previous two reactions (see below).

Comparison of the Various Addition Reactions. The results of the calculations reveal several findings:

(a) The geometrical data suggest that all reactions proceed through an early transition state. In the transition state, the angle between the attacking oxygen in $NO_3^\bullet$ and the C≡C triple bond is ca. 98 ± 5°, where an increasing degree of substitution at the alkyne bond leads to a slight decrease of the attacking angle by a few degrees. Thus, the angle of attack is on the same order of magnitude as in radical additions to alkenes.[33]

(b) The transition state was found to be energetically above the reactants only in the reaction of $NO_3^\bullet$ with ethyne. The negative values for the transition-state energies relative to $NO_3^\bullet$ and alkyne determined in the majority of the computations on the reaction of $NO_3^\bullet$ with propyne and 2-butyne indicate formation of a prereactive complex prior to the actual attack at the π system.[39] For all three reactions under investigation, careful examination of the potential surface, indeed, revealed such prereactive complexes with $NO_3^\bullet$−alkyne distances of more than 2.5 Å (see Figures 2, 4, and 5), which are lower in energy than the corresponding reactants by few kilojoules per mole. Calculation of the energy difference between complex and respective transition states led to the expected positive activation barriers $\Delta E^\ddagger$ for all three reactions.

As can be seen from Tables 2−4, the $\Delta E^\ddagger$ data obtained from the QCISD and CCSD(T) single-point calculations are signifi-

cantly higher than those from the DFT computations, with the QCISD results being even higher by up to ca. 10 kJ mol^{-1} compared with the CCSD(T) data. This discrepancy between the QCISD and CCSD(T) outcomes could be due to the doublet nature of the system and the different treatment of monoexcitation terms in both methods. To assess the quality of the wave function, T_1 diagnostics were therefore exemplary performed for the $NO_3^•$−ethyne reaction, which revealed a T_1 value of $\leq$0.036. According to literature,[40] this could be taken as an indication for nondynamical correlation effects which are large enough to render results from single reference methods limited to single and double excitations potentially unreliable. However, the very good agreement between the QCISD, CCSD(T), and BHandHLYP results in calculating the activation energy for the reverse fragmentation of the vinyl radicals into $NO_3^•$ and alkyne, ΔE_3, suggests that the origin of the discrepancy between the DFT and single-point computations in determining $\Delta E^‡$ should be different. Potential uncertainties in these calculations are due to the difficulty of locating the prereactive $NO_3^•$−alkyne association complex on the very shallow potential energy surface in this area, which was used for calculating $\Delta E^‡$.[41] To evaluate the influence of methyl substitution at the C≡C triple bond on the height of the activation barrier, we decided to use an indirect approach. First, the reaction enthalpy, ΔE_2, of all three reactions was examined (considering the angular pathway in the reaction of $NO_3^•$ with ethyne), which turned out to be the same for all three reactions within 10 kJ mol^{-1}, at each level of theory. However, whereas the BHandHLYP calculations reveal no clear trend between ΔE_2 and degree of methyl substitution in the vinyl radicals, the QCISD and CCSD(T) computations show that the reaction of ethyne is the least exothermic (-84 ± 5 kJ mol^{-1}) and the reaction of 2-butyne is the most exothermic (-93 ± 6 kJ mol^{-1}). The small energy difference between the most and least exothermic reactions suggests that methyl substitution has only a minimal impact (ca. 5 kJ mol^{-1} per methyl group) on the stability of vinyl radicals. In contrast to the relatively invariant ΔE_2 value, ΔE_3 gradually decreases in the line ethyne − propyne − 2-butyne by ca. 7 and ca. 15 kJ mol^{-1}, respectively, thus reflecting the difference in activation energy required for the three reactions. On average, increasing methyl substitution at the C≡C triple bond leads to a decrease of the activation barrier by ca. 11 kJ mol^{-1} per methyl substituent. Despite the uncertainty mentioned above, the value of $\Delta E^‡$ largely mirrors this trend and shows that the addition of $NO_3^•$ at 2-butyne has the lowest and the addition of $NO_3^•$ at ethyne the highest activation barrier of the reactions under investigation. A decreasing activation barrier with increasing alkyl substitution can be rationalized by the +I effect of methyl groups, which enhances the electron density at the C≡C triple bond, thus reducing the energy difference between the HOMO of the alkyne and the SOMO of the electrophilic $NO_3^•$. Our computational results are in agreement with gas-phase experiments that showed that increasing alkyl substitution at the C≡C triple bond leads to a faster reaction with $NO_3^•$.[1,23]

(c) Whereas the reaction of $NO_3^•$ with ethyne proceeds via two energetically very close transition states **TS-e(s)** and **TS-e(a)** to two low-energy vinyl radicals ***Z*-e(s)** and ***Z*-e(a)**, only one transition state was located for the reaction of $NO_3^•$ with propyne and 2-butyne, respectively. Steric repulsions that would arise between the attacking $NO_3^•$ and the methyl substituent at C^2 in propyne or 2-butyne may be the reason for the absence of a planar, *syn*-configurated transition state leading to planar *syn* vinyl radicals in these two reactions.

(d) The energy difference between the vinyl radicals ***E*-** and ***Z*-e(s)** or ***E*-** and ***Z*-e(a)**, respectively, formed in the reaction of $NO_3^•$ with ethyne, is with $\leq$1.4 kJ mol^{-1} below the accuracy of the applied computational methods, and we consider them energetically equivalent. Increasing methyl substitution at the π bond leads to a slight stabilization of the corresponding *Z*-configurated vinyl radicals with ***Z*-p** being up to 4.0 kJ mol^{-1} and ***Z*-b** being up to 4.9 kJ mol^{-1} more stable than the respective *E*-configurated radicals.[42] This energy difference is, however, not very large and indicates that both geometrical isomers are existing in equilibrium mixtures (***E*/*Z*-p** and ***E*/*Z*-b**) at room temperature.

Conclusions

We have shown in this study that the outcome of $NO_3^•$ geometry calculations using DFT methods strongly depends on the degree of HF exchange in the hybrid density functionals. Although in no case was spatial symmetry breaking of the wave function observed, only B3LYP results in the correct D_{3h} symmetry as the energy minimum for $NO_3^•$. Computations using the mPW1PW91 hybrid functional lead to the incorrect inverted C'_{2v} geometry, whereas C_{2v} and D_{3h} symmetries appear as a transition state or a second-order saddle point, respectively. Generally, hybrid functionals with HF exchange of more than 40%, e.g., mPW1K and BHandHLYP, continuously show the likewise incorrect C_{2v} geometry as the energy minimum structure of $NO_3^•$, whereas D_{3h} symmetric $NO_3^•$ was only found as a saddle point of second order.

The $NO_3^•$ addition to ethyne, propyne, and 2-butyne was studied using various ab initio and DFT methods in combination with different basis sets. These reactions are proceeding through early, *Z*-configurated transition states leading to *Z*-configurated vinyl radicals that may subsequently undergo *Z*/*E* isomerization. Intermediate prereactive $NO_3^•$−alkyne complexes have been located for all three reactions. Ethyne has an exceptional position in this series of alkynes, as two different transition states and two pairs of *E*/*Z* isomeric vinyl radicals were found, whereas only one transition state could be located in the addition of $NO_3^•$ to propyne and 2-butyne, leading to one pair of *E*/*Z* isomeric vinyl radicals in each case. Besides the angular $NO_3^•$ approach to the C≡C triple bond found in all three reactions, absence of steric hindrance in ethyne also enables a *syn* periplanar arrangement of $NO_3^•$ and the C≡C triple bond in the transition state leading to the planar, *syn*-configurated vinyl radicals ***E*/*Z*-e(s)**. The angle of $NO_3^•$ attack at the triple bond is with ca. 98 $\pm$ 5° in the same order of magnitude as in radical additions to alkenes. All reactions are strongly exothermic, but the effect of methyl substitution on the stabilization of vinyl radicals is relatively small, with ca. 5 kJ mol^{-1} per methyl group. The activation barrier of the radical addition decreases with increasing degree of substitution at the alkyne bond by ca. 11 kJ mol^{-1} per methyl substituent.

The calculations revealed some dependencies of the applied level of theory on the outcome in terms of both geometry and energy of transition and ground state structures. Comparison of the results obtained from single-point calculations using electron correlating methods [CCSD(T) and QCISD] revealed good agreement with computations performed at the BHandHLYP/cc-pVDZ level of theory. Larger basis sets in combination with the BHandHLYP method did not seem to dramatically change the relative energy differences and geometries of the various species. In contrast to this, both the UHF method and DFT methods using hybrid functionals with lower HF exchange than in BHandHLYP turned out to be unsuitable for the study

of this radical addition reaction. The moderate computational resources that BHandHLYP/cc-pVDZ calculations are requiring will enable us now to investigate the entire mechanism of self-terminating, oxidative radical cyclizations.

Acknowledgment. We thank Professor Carl H. Schiesser, The University of Melbourne, for his invaluable support. Financial support by the Studienstiftung des Deutschen Volkes, Deutscher Akademischer Austauschdienst, Stipendienstiftung der Universität Kiel, Deutsche Forschungsgemeinschaft and The University of Melbourne is gratefully acknowledged. We thank the Rechenzentrum der Universität Kiel, the Advanced Research Computing Centre of the University of Melbourne, and the Victorian Institute for Chemical Sciences High Performance Computing Facility for support.

Supporting Information Available: (a) Mechanistic scheme of a self-terminating radical oxygenation. (b) $NO_3^{\bullet}$: Table with Mulliken charges, dipole moments, electronic energies and the remaining harmonic frequencies for $NO_3^{\bullet}$. (c) $NO_3^{\bullet}$ addition to alkynes: Tables with the electronic energies, $\langle s^2 \rangle$ values, imaginary frequencies, ν_{imag}, for transition states and selected geometrical parameters for all structures. This material is available free of charge via the Internet at http://pubs.acs.org.

References and Notes

(1) See for example: Wayne, R. P.; Barnes, I.; Biggs, P.; Burrows, J. P.; Canosa-Mas, C. E.; Hjorth, J.; Le Bras, G.; Moortgat, G. K.; Perner, D.; Restelli, G.; Sidebottom, H. The Nitrate Radical: Physics, Chemistry and the Atmosphere. *Atmos. Environ.* **1991**, *A25*; and cited references.

(2) (a) Wille, U.; Plath, C. *Liebigs Ann./Recueil* **1997**, 111. (b) Wille, U.; Lietzau, L. *Tetrahedron* **1999**, *55*, 10119. (c) Wille, U.; Lietzau, L. *Tetrahedron* **1999**, *55*, 11465. (d) Lietzau, L.; Wille, U. *Heterocycles* **2001**, *55*, 377. (e) Wille, U. *Chem.—Eur. J.* **2002**, *8*, 340. (f) Dreessen, T.; Jargstorff, C.; Lietzau, L.; Plath, C.; Stademann, A.; Wille, U. *Molecules* **2004**, *9*, 480. (g) Stademann, A.; Wille, U. *Aust. J. Chem.* **2004**, *57*, 1055.

(3) A mechanistic scheme for a typical self-terminating radical oxygenation is given in the electronic Supporting Information.

(4) The calculations of the remaining reaction steps of the self-terminating radical oxygenation sequence will be presented separately: Dreessen, T.; Wille, U. Unpublished results.

(5) (a) Olsen, J. F.; Burnelle, L. *J. Am. Chem. Soc*. **1970**, *92*, 3659. (b) Baird, N. C.; Taylor, K. F. *Chem. Phys. Lett*. **1981**, *80*, 83. (c) Kim, B.; Johnston, H. S.; Clabo, D. A., Jr.; Schaefer, H. F., III *J. Chem. Phys*. **1988**, *88*, 3204. (d) Boehm, R. C.; Lohr, L. L. *J. Phys. Chem*. **1989**, *93*, 3430. (e) Boehm, R. C.; Lohr, L. L. *J. Comput. Chem*. **1991**, *12*, 119. (f) Davy, R. D.; Schaefer, H. F., III *J. Chem. Phys*. **1989**, *91*, 4410. (g) Kim, B.; Hammond, B. L.; Lester, W. A., Jr.; Johnston, H. S. *Chem. Phys. Lett*. **1990**, *168*, 131. (h) Morris, V. R.; Bhatia, S. C.; Hall, J. H., Jr. *J. Phys. Chem*. **1990**, *94*, 7414. (i) Morris, V. R.; Bhatia, S. C.; Hall, J. H., Jr. *J. Phys. Chem.* **1991**, *95*, 9203.

(6) (a) Kim, B.; Hunter, P. L.; Johnston, H. S. *J. Chem. Phys.* **1992**, *96*, 4057. (b) Friedl, R. R.; Sander, S. P. *J. Phys. Chem*. **1987**, *91*, 2721. (c) Ishiwata, T.; Tanaka, I.; Kawaguchi, K.; Hirota, E. *J. Chem. Phys*. **1985**, *82*, 2196. (d) Kawaguchi, K.; Hirota, E.; Ishiwata, T.; Tanaka, I. *J. Chem. Phys*. **1990**, *93*, 951. (e) Kawaguchi, K.; Ishiwata, T.; Tanaka, I.; Hirota, E. *Chem. Phys. Lett*. **1991**, *180*, 436. (f) Kawaguchi, K.; Ishiwata, T.; Hirota, E.; Tanaka, I. *Chem. Phys.* **1998**, *231*, 193. (g) Ishiwata, T.; Tanaka, I.; Kawaguchi, K.; Hirota, E. *J. Mol. Spectrosc.* **1992**, *153*, 167. (h) Weaver, A.; Arnold, D. W.; Bradford, S. E.; Neumark, D. M. *J. Chem. Phys.* **1991**, *94*, 1740. (i) Monks, P. S.; Stief, L. J.; Krauss, M.; Kuo, S. C.; Zhang, Z.; Klemm, R. B. *J. Phys. Chem*. **1994**, *98*, 10017. (j) Wang, D.; Jiang, P.; Qian, X.; Hong, G. *J. Chem. Phys*. **1997**, *106*, 3003.

(7) Symmetry breaking is an artifact caused by an inadequately approximated solution of the electronic Schrödinger equation and is frequently encountered in computations of highly symmetric open-shell molecules; see for example: (a) McLean, A. D.; Lengsfeld, B. H., III; Pacansky, J.; Ellinger, Y. *J. Chem. Phys*. **1985**, *83*, 3567. (b) Sherill, C. D.; Lee, M. S.; Head-Gordon, M. *Chem. Phys. Lett*. **1999**, *302*, 425. (c) Cohen, R. D.; Sherill, C. D. *J. Chem. Phys.* **2001**, *114*, 8257.

(8) Eisfeld, W.; Morokuma, K. *J. Chem. Phys*. **2000**, *113*, 5587.

(9) (a) Stirling, A.; Pápai, I.; Mink, J.; Salahub, D. R. *J. Chem. Phys*. **1994**, *100*, 2910. (b) Munakata, H.; Kakumoto, T.; Baker, J. *THEOCHEM* **1997**, *391*, 231. (c) Aplincourt, P.; Bohr, F.; Ruiz-Lopez, M. F. *THEOCHEM* **1998**, *426*, 95.

(10) Slater, J. C. *Quantum Theory of Molecular and Solids. Vol. 4: The Self-Consistent Field for Molecular and Solids*; McGraw-Hill: New York, 1974.

(11) Vosko, S. H.; Wilk, L.; Nusair, M. *Can. J. Phys.* **1980**, *58*, 1200.

(12) Becke, A. D. *Phys. Rev. A* **1988**, *38*, 3098.

(13) Lee, C.; Yang, W.; Parr, R. G. *Phys. Rev. B* **1988**, *37*, 785.

(14) Perdew, J. P. *Phys. Rev. B* **1986**, *33*, 8822.

(15) Perdew, J. P.; Wang, Y. *Phys. Rev. B* **1992**, *45*, 13244.

(16) Davis, H. F.; Kim, B.; Johnston, H. S.; Lee, Y. T. *J. Phys. Chem.* **1993**, *97*, 2172.

(17) Becke, A. D. *J. Chem. Phys.* **1993**, *98*, 5648.

(18) Truong, T. N.; Duncan, W. *J. Chem. Phys.* **1994**, *101*, 7408.

(19) Frisch, A.; Frisch, M. J. *Gaussian 98 Users Reference*; Gaussian Inc.: Pittsburgh, PA, 1998.

(20) (a) Perdew, J. P. In *Electronic Structure of Solids '91*; Ziesche, P., Eschrig, H., Eds.; Akademie Verlag: Berlin, 1991. (b) Perdew, J. P.; Chevary, J. A.; Vosko, S. H.; Jackson, K. A.; Pederson, M. E.; Singh, D. J.; Fiolhais, C. *Phys. Rev. B* **1992**, *46*, 6671. (c) Perdew, J. P.; Chevary, J. A.; Vosko, S. H.; Jackson, K. A.; Pederson, M. R.; Singh, D. J.; Fiolhais, C. *Phys. Rev. B* **1993**, *48*, 4978. (d) Burke, K.; Perdew, J. P.; Wang, Y. In *Electronic Density Functional Theory: Recent Progress and New Directions*; Dobson, J. F., Vignale, G., Das, M. P., Eds.; Plenum: New York, 1998. (e) Perdew, J. P.; Burke, K.; Wang, Y. *Phys. Rev. B* **1996**, *54*, 16533. (f) Adamo, C.; Barone, V. *J. Chem. Phys*. **1998**, *108*, 664.

(21) The mPW1K functional was optimized for hydrogen abstraction reactions; see for example: Lynch, B. J.; Fast, P. L.; Harris, M.; Truhlar, D. G. *J. Phys. Chem. A* **2000**, *104*, 4811.

(22) (a) Pérez-Casany, M. P.; Nebot-Gil, I.; Sánchez-Martin, J.; Thomás-Vert, F.; Martínez-Ataz, E.; Cabañas-Galán, B.; Aranda-Rubio, A. *J. Org. Chem.* **1999**, *63*, 6987. (b) Cartas-Rosado, R.; Santoyo, M. E. R.; Alvarez-Idaboy, J. R.; Vivier-Bunge, A. *J. Phys. Chem. A* **2001**, *105*, 9222. (c) Pérez-Casany, M. P.; Nebot-Gil, I.; Sánchez-Martin, J. *J. Phys. Chem. A* **2000**, *104*, 6277. (d) Pérez-Casany, M. P.; Nebot-Gil, I.; Sánchez-Martin, J. *J. Phys. Chem. A* **2000**, *104*, 10721. (e) Pérez-Casany, M. P.; Nebot-Gil, I.; Sánchez-Martin, J. *J. Phys. Chem. A* **2000**, *104*, 11340. (f) Pérez-Casany, M. P.; Sánchez-Martin, J.; Nebot-Gil, I. *J. Am. Chem. Soc.* **2000**, *122*, 11585.

(23) (a) Atkinson, R. *J. Phys. Chem. Ref. Data* **1991**, *20*, 459. (b) Canosa-Mas, C. E.; Smith, S. J.; Toby, S.; Wayne, R. P. *J. Chem. Soc., Faraday Trans. 2* **1988**, *84*, 247. (c) Canosa-Mas, C. E.; Smith, S. J.; Toby, S.; Wayne, R. P. *J. Chem. Soc., Faraday Trans. 2* **1988**, *84*, 263. (d) Benter, T.; Becker, E.; Wille, U.; Schindler, R. N.; Canosa-Mas, C. E.; Smith, S. J.; Waygood, S. J.; Wayne, R. P. *J. Chem. Soc., Faraday Trans. 2* **1991**, *87*, 2141. (e) Seland, J. G.; Noremsaune, I. M. W.; Nielsen, C. J. *J. Chem. Soc., Faraday Trans.* **1996**, *92*, 3459. (f) Atkinson, R.; Aschmann, S. M.; Goodman, M. A. *Int. J. Chem. Kinet.* **1987**, *19*, 299.

(24) (a) Frisch, M. J.; Trucks, G. W.; Schlegel, H. B.; Scuseria, G. E.; Robb, M. A.; Cheeseman, J. R.; Zakrzewski, V. G.; Montgomery, J. A., Jr.; Stratmann, R. E.; Burant, J. C.; Dapprich, S.; Millam, J. M.; Daniels, A. D.; Kudin, K. N.; Strain, M. C.; Farkas, O.; Tomasi, J.; Barone, V.; Cossi, M.; Cammi, R.; Mennucci, B.; Pomelli, C.; Adamo, C.; Clifford, S.; Ochterski, J.; Petersson, G. A.; Ayala, P. Y.; Cui, Q.; Morokuma, K.; Malick, D. K.; Rabuck, A. D.; Raghavachari, K.; Foresman, J. B.; Cioslowski, J.; Ortiz, J. V.; Stefanov, B. B.; Liu, G.; Liashenko, A.; Piskorz, P.; Komaromi, I.; Gomperts, R.; Martin, R. L.; Fox, D. J.; Keith, T.; Al-Laham, M. A.; Peng, C. Y.; Nanayakkara, A.; Gonzalez, C.; Challacombe, M.; Gill, P. M. W.; Johnson, B. G.; Chen, W.; Wong, M. W.; Andres, J. L.; Head-Gordon, M.; Replogle, E. S.; Pople, J. A. *Gaussian 98*, revision A.11.4; Gaussian, Inc.: Pittsburgh, PA, 2002. (b) Frisch, M. J.; Trucks, G. W.; Schlegel, H. B.; Scuseria, G. E.; Robb, M. A.; Cheeseman, J. R.; Zakrzewski, V. G.; Montgomery, J. A., Jr.; Stratmann, R. E.; Burant, J. C.; Dapprich, S.; Millam, J. M.; Daniels, A. D.; Kudin, K. N.; Strain, M. C.; Farkas, O.; Tomasi, J.; Barone, V.; Cossi, M.; Cammi, R.; Mennucci, B.; Pomelli, C.; Adamo, C.; Clifford, S.; Ochterski, J.; Petersson, G. A.; Ayala, P. Y.; Cui, Q.; Morokuma, K.; Malick, D. K.; Rabuck, A. D.; Raghavachari, K.; Foresman, J. B.; Cioslowski, J.; Ortiz, J. V.; Stefanov, B. B.; Liu, G.; Liashenko, A.; Piskorz, P.; Komaromi, I.; Gomperts, R.; Martin, R. L.; Fox, D. J.; Keith, T.; Al-Laham, M. A.; Peng, C. Y.; Nanayakkara, A.; Gonzalez, C.; Challacombe, M.; Gill, P. M. W.; Johnson, B. G.; Chen, W.; Wong, M. W.; Andres, J. L.; Head-Gordon, M.; Replogle, E. S.; Pople, J. A. *Gaussian 98*, revision A.7; Gaussian, Inc.: Pittsburgh, PA, 1998. (c) Frisch, M. J.; Trucks, G. W.; Schlegel, H. B.; Gill, P. M. W.; Johnson, B. G.; Robb, M. A.; Cheeseman, J. R.; Keith, T.; Petersson, G. A.; Montgomery, J. A.; Raghavachari, K.; Al-Laham, M. A.; Zakrzewski, V. G.; Ortiz, J. V.; Foresman, J. B.; Cioslowski, J.; Stefanov, B. B.; Nanayakkara, A.; Challacombe, M.; Peng, C. Y.; Ayala, P. Y.; Chen, W.; Wong, M. W.; Andres, J. L.; Replogle, E. S.; Gomperts, R.; Martin, R. L.; Fox, D. J.; Binkley, J. S.; Defrees, D. J.; Baker, J.; Stewart, J. P.; Head-Gordon, M.; Gonzalez, C.; Pople, J. A. *Gaussian 94*, revision D.4/E.2; Gaussian, Inc.: Pittsburgh, PA, 1995.

(25) This energy difference is lesser than the precision that normally is assigned to the theoretical methods.

(26) Crawford, T. D.; Stanton, J. F. *J. Chem. Phys.* **2000**, *112*, 7873.

(27) Janoschek, R.; Kalcher, J. *Z. Anorg. Allg. Chem.* **2002**, *628*, 2724.

(28) In our computations, basis sets with diffuse functions generally resulted in higher absolute values for the atomic charges and dipole moments (see Supporting Information).

(29) $\Delta_f H°$ was determined according to: Ochterski, J. W. http://www.gaussian.com/g_whitepap/thermo.htm (Accessed 2000).

(30) Additional conformers of the vinyl radicals and transition states resulting from rotation along the C−O bond were also located, but since they were higher in energy by few kJ mol^{-1}, they were not further considered.

(31) Since this supermolecule is not symmetric at all, no symmetry breaking problems should appear.

(32) Curran, D. P.; Porter, N. A.; Giese, B. *Stereochemistry of Radical Reactions*; VCH: Weinheim, 1996.

(33) No attempt was made in this work to locate the transition state of the *Z*/*E* isomerization of the vinyl radicals because of the expected low activation barrier and its insignificance for the course of the radical oxygenation cascade; see also: Fossey, J.; Lefort, D.; Sorba, J. *Free Radicals in Organic Chemistry*; John Wiley & Sons: Chichester, 1995.

(34) We refrained from using experimentally determined activation barriers for the addition of $NO_3^\bullet$ to alkynes to benchmark our computational results. The rates of these reactions are on the lower limit accessible by the fast-flow techniques that were used for their determination, and the obtained data are consequently afflicted with significant errors; see refs 1 and 23a−d.

(35) The B3LYP method is well-known to underestimate the size of activation barriers in radical reactions; see ref 22b.

(36) Because radical addition preferably occurs at the less-hindered site, $NO_3^\bullet$ attack at the higher substituted site of the C≡C triple bond was not investigated; see ref 22c and: (a) Vereecken, L.; Peeters, J.; Bettinger, H. F.; Kaiser, R. I., Schleyer, P. v. R.; Schaefer, H. F., III *J. Am. Chem. Soc.* **2002**, *124*, 2781. (b) Fischer, H.; Radom, L. *Angew. Chem., Int Ed.* **2001**, *40*, 1340.

(37) Structures with a $\theta_{NOC^1C^2}$ of ca. 180° were located as transition states of the rotation between the two enantiomers of ***E*-p** and ***Z*-p**, respectively (not shown).

(38) The addition of $NO_3^\bullet$ to both propyne and 2-butyne was also calculated using the UHF, B3LYP, mPW1PW91, and mPW1K methods as shown in Table 2 (see Supporting Information). Comparison with the results of the single-point computations at correlated levels showed a poorer performance of these methods similar to the findings in the reaction of $NO_3^\bullet$ with ethyne.

(39) The transition-state energies relative to $NO_3^\bullet$ and alkyne are not given in Tables 2−4, but can be calculated from the difference $\Delta E^\ddagger - \Delta E_1$.

(40) Lee, T. J.; Head-Gordon, M.; Rendell, A. P. *Chem. Phys. Lett.* **1995**, *243*, 402.

(41) This might be because DFT methods cannot reproduce intermolecular interactions well. The calculated geometries for **complex-e/p/b** showed indeed the largest dependencies on the theoretical level of theory used in this work (see Supporting Information).

(42) Similar to our results, it was found that addition of methyl and phenyl radicals to ethyne or propyne leads, via *Z*-configurated transition states, to *Z*-configurated vinyl radicals; see refs 36a and: Gómez-Balderas, R.; Coote, M. L.; Henry, D. J.; Fischer, H.; Radom, L. *J. Phys. Chem. A* **2003**, *107*, 6082.